Determining Irrigated Areas and Quantifying Blue Water Use in Europe Using Remote Sensing Meteosat Second Generation (MSG) products and Global Land Data Assimilation System (GLDAS) Data

Mireia Romaguera, Maarten S. Krol, Mhd. Suhyb Salama, Arjen Y. Hoekstra, and Zhongbo Su

Abstract

In this paper, we propose an innovative method for identifying irrigated areas and quantifying the blue evapotranspiration (ET_b), or irrigation water evapotranspired from the field. The method compares actual ET (ET_{actual}), or crop water use, values from the Global Land Data Assimilation System (GLDAS) and remote sensing based ET_{actual} estimates obtained from Meteosat Second Generation (MSG) satellites. Since GLDAS simulations do not account for extra water supply due to irrigation, it is expected that they underestimate ET_{actual} during the cropping season in irrigated areas. However, remote sensing techniques based on the energy balance are able to observe the total ET_{actual}. In order to isolate irrigation effects from other fluctuations that may lead to discrepancies between the different ET_{actual} products, the bias between model simulations and remote sensing observations was estimated using reference targets of rainfed (non-irrigated) croplands on a daily basis in different areas across the study region (Europe). Analysis of the yearly values of ET_b (irrigated area and volume obtained for croplands in Europe for 2008) showed that the method identified irrigation when yearly values were higher than 50 mm. The accuracy of the method was assessed by analyzing the spatial representativity of the calculated biases and evaluating the daily ET_b values obtained. The irrigated areas were compared with the results provided by Siebert et al.(2007) and Thenkabail et al.(2009b), obtaining a spatial match of 47 and 72 percent, respectively, with overestimation of irrigated area on a country scale. Additional evaluation with the ET_b results of Mekonnen and Hoekstra (2011) showed 75 percent of overlap for ±50 mm range. Finally, validation with in situ data on irrigation volumes proved the cogency of our method with less than 20 percent difference between derived and measured values.

Introduction

Monitoring and quantification of irrigation practices play an important role in water management activities and global water resources since water is becoming a scarce but essential resource.

In this context, the concept of actual evapotranspiration (ET_{actual}) has been widely used to assess the usage of water resources and irrigation practices by using ground based and/or remote sensing data (D'Urso *et al.*, 2008; Gowda *et al.*, 2008). These studies have been focused on predicting the optimal irrigation supply based on the crop water demand. Other works have established the difference between the blue and green components of ET_{actual}, that is the irrigation and precipitation water usage (Mekonnen and Hoekstra, 2010; Siebert and Döll, 2010).

Irrigation practices influence water availability for evapotranspiration and ET_{actual} at regional scale, which is also reflected in the partitioning of energy between sensible and latent heat flux. As an example, Ozdogan *et al.* (2010) simulated the effects of including irrigation as an extra water supply in the Noah land surface model (Chen *et al.*, 1996; Koren *et al.*, 1999) and showed that the increment in daily ET_{actual} reached up to 5 mm/day in extreme situations in the United States. Noah is based on the energy and water conservation laws and is forced by precipitation among others. It is a budget based land surface model that does not account for irrigation practices.

In the validation report LSA-SAF (2010b), the Global Land Data Assimilation System (GLDAS) ET_{actual} products generated with Noah, named GLDAS-ET in the following, are compared with the remote sensed ET_{actual} estimates obtained from Meteosat Second Generation (MSG) satellites (Gellens-Meulenberghs *et al.*, 2007), named MSG-ET in the following.

Mireia Romaguera is with the Faculty of Engineering Technology, Department of Water Engineering and Management, and the Faculty of Geo-Information Science and Earth Observation, Department of Water Resources, University of Twente, NL-7500 AE Enschede, The Netherlands (romaguera@itc.nl).

Maarten S. Krol and Arjen Y. Hoekstra are with the Faculty of Engineering Technology, Department of Water Engineering and Management, University of Twente, NL-7500 AE Enschede, The Netherlands.

Mhd. Suhyb Salama and Zhongbo Su are with the Faculty of Geo-Information Science and Earth Observation, Department of Water Resources, University of Twente, NL-7500 AA Enschede, The Netherlands.

Photogrammetric Engineering & Remote Sensing
Vol. 78, No. 8, August 2012, pp. 861–873.

0099-1112/12/7808–861/$3.00/0

The latter model is based on the physical processes that occur and the inputs are taken from remote sensing retrievals. This comparison shows some differences in several areas especially during summer periods. The authors justify these discrepancies by analyzing the differences in the inputs used in the two models, but no reference is made to the fact that the Noah model does not account for irrigation practices which may lead to the ET_{actual} differences that are found along Europe, Africa, and South America. The comparison in the aforementioned work was carried out at continental scale in a statistical manner by using temporal and/or spatial averages which does not allow extracting more detailed information about the seasonality and spatial variation of these differences.

Therefore, the objective of this paper is to compare the ET_{actual} outputs of the two aforementioned models, GLDAS-ET and MSG-ET, at a daily and grid base with continental coverage, by assuming that the discrepancies are partly due to the fact that irrigation (or blue evapotranspiration, ET_b) is only represented in the MSG-ET model. This allows determining irrigated areas and comparing with existing irrigation maps such as the ones obtained by Siebert *et al.* (2007) and Thenkabail *et al.* (2009b). Moreover, volumes of ET_b may be contrasted with the blue water footprint calculations by Mekonnen and Hoekstra (2011).

The next Section of this paper describes the datasets used and the physical background of the two models; then methodology is explained. In order to isolate the irrigation effects from other sources of differences, such as modeling, type of inputs or scale issues, rainfed croplands are used to calculate a spatially-dependent reference bias between the models. Based on the analysis of the inputs of the two models and some previous analysis carried out at LSA-SAF (2010b), the MSG observation geometry and the Normalized Difference Vegetation Index (NDVI) and its seasonality appear to be factors that contribute to explain the discrepancies between the models. Therefore, the bias is defined as a function of the MSG viewing zenith angle, maximum value of the NDVI and the season where NDVI is maximum. In the Results Section a classification map is produced with a total of 12 reference biases in Europe, and ET_b is calculated in 2008. The assessment of the accuracy of the method is included in this section. The final Section compares the obtained irrigated areas with the irrigation maps given by Siebert *et al.* (2007) and Thenkabail *et al.* (2009b), at pixel scale and country aggregated. Additionally, volumes of ET_b are compared with the results given by Mekonnen and Hoekstra (2011), and *in situ* values of irrigation are used to compare with downscaled ET_b values at point scale.

Data Sets

The main datasets used in this research are the ET_{actual} obtained from MSG satellites (MSG-ET) and the ET_{actual} data from the GLDAS dataset (GLDAS-ET). Other inputs are the GlobCover land-cover classification (UCLouvain and ESA, 2011), the NDVI dataset generated by the Deutsches Zentrum für Luft- und Raumfahrt (DLR), and the MSG viewing zenith angle (VZA). In order to evaluate the accuracy of the proposed method, the results are compared with the Global Map of Irrigation Areas (Siebert *et al.*, 2005), the Global Irrigated Area Map (Thenkabail *et al.*, 2009b), and the blue Water Footprint results given by Mekonnen and Hoekstra (2011). Table 1 shows the main specifications of these data.

From a technical point of view, the combination of data with different spatial resolution, extent and projection was tackled by creating a layer stack where the data were resampled and re-projected to a common output projection and pixel size. The classification map was created at a resolution of 1 km. The reference biases were calculated in rainfed pixels using data at 300 m in order to preserve the resolution of the GlobCover map. Finally, the ET_b outputs were obtained at 1 km resolution and rescaled to 5 arc-minutes in order to compare with the existing maps.

MSG-ET Data

The ET_{actual} products from the MSG satellites are provided by the Land Surface Analysis Satellite Applications Facility (LSA-SAF) at a resolution of 3 km at sub-nadir point which increases with the satellite observation angle, and a temporal frequency of 30 minutes. These data cover the continents of Europe and Africa and partly South-America and are available since January 2007 for Europe and September 2009 for the rest.

The methodology to retrieve ET_{actual} is based on the physical processes and exchange of energy between the ground surface (soil and canopy) and the atmosphere, and uses inputs derived from the MSG satellites.

TABLE 1. SPECIFICATIONS OF THE DATASETS USED IN THIS PAPER

Data	Source	Spatial coverage	Spatial resolution	Temporal resolution	Details
ET_{actual}	MSG	MSG disk*	3 km at nadir	30'	Availability of data: Europe: Jan. 2007 to present The rest: Sept. 2009-present
	GLDAS	Global	0.25° (~30 km at equator)	3h	Availability of data: February 2000 to present
Classification	MERIS	Global	300 m	Static	GlobCover map calculated in year 2009
NDVI	AVHRR	Europe	1 km	Monthly	Composites obtained in year 1997
VZA	MSG	MSG disk*	5 arc-min (~10 km at equator)	Static	Range: 0 to 90°
Irrigation	GMIA	Global	5 arc-min (~10 km at equator)	Static	(Siebert *et al.*, 2007) Calculated around year 2000 Data: % of irrigated area
	GIAM				(Thenkabail *et al.*, 2009b) Calculated around year 1999 Data: Type of Irrigation
	Blue WF				Mekonnen and Hoekstra (2011) Data: blue WF per year

*Meteosat disk covers latitudes between −60° and +60° and longitudes between −60° to +60°.
**List of acronyms: MSG (Meteosat Second Generation), GLDAS (Global Land Data Assimilation System), MERIS (Medium Resolution Imaging Spectrometer), AVHRR (Advanced Very High Resolution Radiometer), GMIA (Global Map of Irrigated Areas), GIAM (Global Irrigation Area Map), WF (Water Footprint).

The method is based on forcing a Soil-Vegetation-Atmosphere-Transfer (SVAT) scheme with relevant data (short and long-wave radiation fluxes ($S\downarrow$and $L\downarrow$), surface albedo (α), leaf area index (LAI), fraction of vegetation cover (FVC) and snow cover) derived from Meteosat and auxiliary data (air temperature, specific humidity, wind speed, atmospheric pressure, etc.) from other sources, i.e., mainly from the European Center for Medium-Range Weather Forecast (ECMWF) (Gellens-Meulenberghs *et al.*, 2007). It is an energy balance model aiming to compute the partition of net radiation (*Rn*) into sensible heat flux (*H*), latent heat flux (*LE*) and heat conduction flux into the ground (*G*) according to:

$$R_n - H - LE - G = 0 \quad (1)$$

The computations are carried out at tile level and an iteration method is needed to solve the involved equations. A gap filling procedure is implemented in pre-processing when $S\downarrow$ is not available and in post-processing when ET_{actual} cannot be calculated because of missing input variables or no convergence of the algorithm (LSA-SAF, 2010a). This process allows generating ET_{actual} products including cloudy pixels.

In the research presented, daily MSG-ET values were obtained by temporal integration of the 48 instantaneous values per day, during the year 2008. Linear interpolation in time was used to fill in missing data, due to non-acquisitions. Daily ET_{actual} values were not considered if missing data occurred during periods of one hour or longer. In general terms, the daily ET_{actual} was calculated for 85 percent of the days along the year 2008, and for 94 percent if the five month period May to September was considered.

Additional data from 2009 were used to test the method with *in situ* data, for which MSG-ET data were acquired between 10 July and 08 September. Daily ET_{actual} was obtained for the 89 percent of the days in this case.

GLDAS-ET Data

The GLDAS datasets are available from the NASA Goddard Earth Sciences Data and Information Services Center (GES DISC) (*http://disc.sci.gsfc.nasa.gov/hydrology/data-holdings*). The system ingests satellite and ground-based observational data products and uses land surface modeling and assimilation techniques in order to generate optimal fields of land surface states and fluxes (Rodell *et al.*, 2004). The GLDAS data used in this paper are generated with the Noah land surface model (Chen *et al.*, 1996; Koren *et al.*, 1999) at a resolution of 0.25° and a temporal frequency of three hours. These data cover the whole globe since February 2000. The model is based on the principles of water and energy conservation laws, in particular, the water budget is formulated by:

$$\frac{dW}{dt} = P - ET_{actual} - Q \quad (2)$$

where dW/dt is the change in the total water storage within a time period (dt) [mm], P is the amount of precipitation within a time period [mm], ET_{actual} is the actual evapotranspiration in a time period [mm], and Q is the total runoff in a time period [mm].

In Noah, the calculation of the fluxes *LE* and *H* start from potential *LE* (*LEp*), based on the soil moisture, atmosphere states, and vegetation characteristics. Constrains to *LEp* are applied resulting in the actual *LE*, which is composed out of three components: direct evaporation from soil, transpiration via plant stomata and evaporation of canopy intercepted water. Input data for these calculations are $S\downarrow$, $L\downarrow$, atmospheric forcings, α, LAI, vegetation parameters, skin temperature, land-cover, soil type, elevation, slope, and precipitation.

In the present research daily ET_{actual} values of GLDAS-ET were obtained by temporal averaging of the eight provided ET_{actual} rates per day. No missing data were found in this dataset.

GlobCover Land Cover Map

The Medium Resolution Imaging Spectrometer (MERIS) GlobCover (ver. 2.3) product for the year 2009 (UCLouvain and ESA, 2011) is a land-cover map produced at a 300 m resolution at a global scale. This map is based on classification techniques by using the surface reflectances observed by the MERIS sensor, and distinguishes 22 cover classes defined with the United Nations Land Cover Classification system (LCCC), among them the post-flooding or irrigated croplands and rainfed croplands. The latter was used in this research. Other classes describe different types and combinations cover types, such as shrublands, forests and grasslands. The idea behind the use of the MERIS product was to profit from the high resolution product as well as generating the irrigation areas and the ET_b based on an independent dataset. This allowed comparing with the irrigation area provided by existing methodologies such as Siebert *et al.* (2007) and Thenkabail *et al.* (2009b).

Monthly NDVI Products

The monthly NDVI products that are employed in this research were generated from the Advanced Very High Resolution Radiometer (AVHRR) by the Deutsches Zentrum für Luft- und Raumfahrt (DLR). They were obtained during the year 1997, in Europe and at a resolution of 1 km (Mucher *et al.*, 2001).

MSG Viewing Zenith Angle

The MSG's are geostationary satellites located at 36,000 km altitude above the Earth. In particular, Meteosat-9, whose products are used in this research, is currently centered at 0° longitude over the Equator. The satellite viewing zenith angle ranges from 0° up to 90° in the edge of the field of view. In the region of Europe, this observation angle is higher than 40°.

Irrigation Maps

Siebert *et al.* (2005) provided a Global Map of Areas equipped for Irrigation (GMIA) with a spatial resolution of 5 arc-minutes, around the year 2000. This method combined sub-national statistical data with land cover information, providing results in terms of percentage of surface area equipped for irrigation.

Thenkabail *et al.* (2009b) developed the Global Irrigated Area Map (GIAM) with 28 classes and a spatial resolution of 10 km, around year 1999. The method is based on classification and identification techniques to establish different classes of irrigated areas and to differentiate irrigated areas from non-irrigated areas, as it was also carried out by Thenkabail *et al.* (2007). Temporal series of remote sensing data were used in this work, such as reflectance values, brightness, temperatures, and NDVI. Precipitation data, a digital elevation model, and a global tree-cover map were also used as input, as well as ground data and Landsat Enhanced Thematic Mapper Plus (ETM+) mosaics. The global map provides classes labeled based on irrigation source (surface water, groundwater, or conjunctive use), intensity (single, double, or continuous crop) and crop dominance. In this paper, an aggregated map with eight

classes which provide watering method, irrigation type, and intensity was used.

Mekonnen and Hoekstra (2011) estimated the global blue and green water footprint (WF), that is, the water consumed for crop production, where blue and green WF stand for irrigation and rain water usage, respectively. In their method, ET_{actual} and irrigation requirements were calculated according to Allen *et al.* (1998) using crop and stress coefficients. The total WF at each grid cell was estimated to be the weighted average of the WFs in a rainfed and an irrigated scenario. The results were averaged between 1996 to 2005 at a resolution of 5 arc-minutes.

Method

Overview

The method to assess irrigation is based on the comparison of the GLDAS-ET and MSG-ET products on a daily base. Differences in ET_{actual} are expected due to differences in forcing inputs, modeling and aggregation of different spatial scales. The idea behind this work is to achieve a major isolation of the modeling part, which as a hypothesis, is related to irrigation influence. Figure 1 shows an example of the comparison carried out during the year 2008 in an irrigated cropland in Spain and in a rainfed cropland area in France, selected using the GlobCover map.

Figure 1 shows how the ET_{actual} estimates differ substantially during the cropping period in the irrigated area, especially during spring and summer seasons. This may be partly due to the additional water supply, which is observed by the remote sensing techniques but it is not modeled in the GLDAS-ET. The two curves in the rainfed cropland have a similar pattern but also show a structural bias in summer. These general patterns are found across the croplands in Europe.

In order to remove the effect of different inputs in the bias between the models, we first refer to the work carried out in the Validation Report of the MSG-ET product at LSA-SAF (2010b). In this report MSG-ET estimates are compared with GLDAS-ET that used the Noah model. In a statistical manner, their results show differences that, according to the authors, are associated to the differences in the inputs of $S\downarrow$, the ratio between LAI and the stomatal resistance (Rs), and land-cover type. However, no mention is given to the possible extra water supply in form of irrigation. In the aforementioned work, $S\downarrow$ appears to be the factor that influences these differences primarily in Europe, especially during spring and summer, where instantaneous values show differences between 15 to 30 percent. The influence of the ratio LAI/Rs shows a seasonality with local maxima around the months of April and June/July. Finally, they show that land-cover differences are quite spatially limited and play a smaller role. The results of this work are spatial and/or temporal integrated and therefore more detailed information about the differences along the year in a particular area cannot be directly extracted.

Here we propose to calculate for rainfed croplands (non-irrigated) a reference bias evapotranspiration ($bias_{ET}$), defined as the difference between MSG-ET and GLDAS-ET on a daily base, that allows removing the effects of the input differences when comparing the ET_{actual} products. Spatial variability needs to be considered when defining the reference bias, since different areas show different curves along the year. As an example, Figure 2 shows the bias in two rainfed pixels located in Spain and the Ukraine, selected using the GlobCover map.

The bias in the region of Spain reaches local maxima around the days 90 and 180, and the maximum amplitude of the bias is around 2 mm/day during summer time. However, the bias in the region of Ukraine reaches local maxima around the days 90 and 215, thus the summer peak is shifted with respect to the area in Spain. Moreover, the amplitude of the bias reaches values up to 4.5 mm/day.

Taking these issues into consideration, together with the fact that the final objective is to generate outputs at a large scale, this work proposes to generate a classification map based on criteria that allow parameterizing the bias obtained in different areas.

Classification Map

The selection of the criteria for the classification was based on the results obtained at the validation report LSA-SAF (2010b) and some additional model input analysis. As previously explained in, differences in $S\downarrow$ and LAI/Rs appear to explain the discrepancies between GLDAS-ET and MSG-ET products according to LSA-SAF (2010b). In the present work, the criteria selected for the classification were the MSG viewing zenith angle (VZA), the season where NDVI reaches the maximum value (t_{max}), and the maximum value of NDVI ($NDVI_{max}$). These aspects are explained and justified in the following.

An analysis was carried out to identify the differences in the inputs of the two models. In both methods, atmospheric

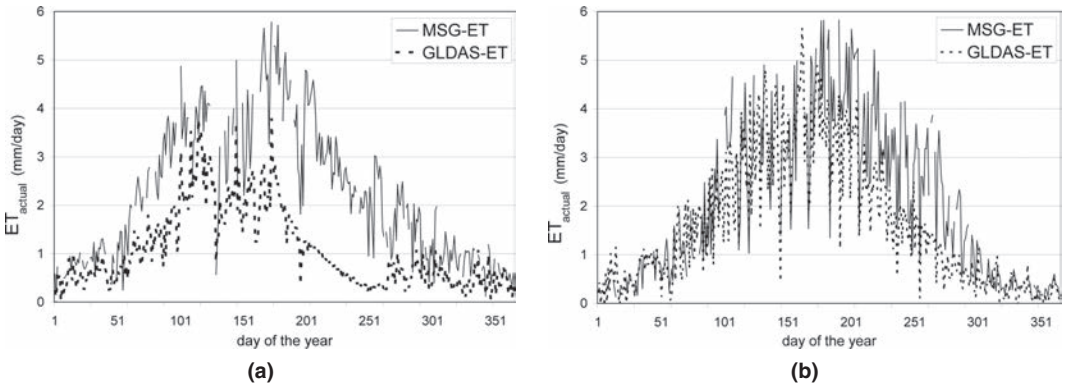

Figure 1. Comparison of MSG-ET and GLDAS-ET in (a) an irrigated cropland in Spain, and (b) rainfed cropland in France.

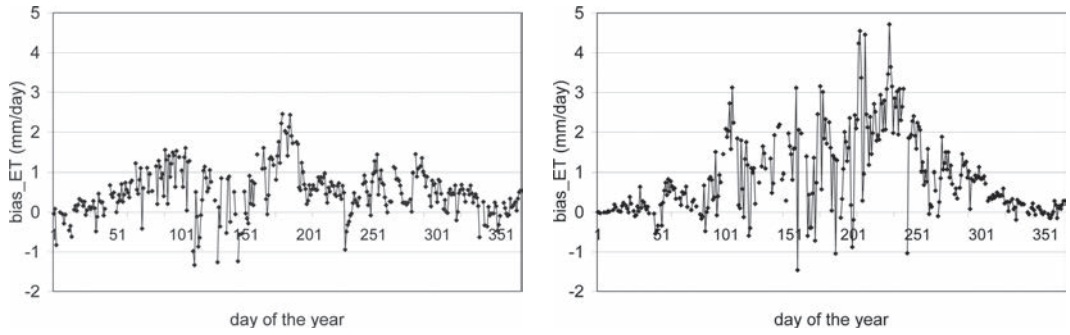

Figure 2. Bias between MSG-ET and GLDAS-ET in two rainfed areas in (a) Spain (42°17′25′′N, 04°58′5′′W), and (b) Ukraine (48°57′25′′N, 34°52′25′′E) during 2008.

forcing is taken from models such as the ECMWF. Regarding the radiative inputs, $S\downarrow$ and $L\downarrow$ are modeled based on the cloud cover and type. The cloud mask used by the MSG products is based on thresholds applied to the channels of the sensor on board the geostationary MSG (NWC-SAF, 2010). However, the cloud information in the $S\downarrow$ of GLDAS-ET incorporates both geostationary and polar-orbiting observations (Rodell *et al.*, 2004). This means that there is a difference in the data in terms of geometry of observation. The products obtained from MSG (ET_{actual}, $S\downarrow$, cloud mask) are more influenced by a VZA, which reaches values up to 90°. The pixel size increases with the observation angle, and the accuracy of the estimates decreases because the atmospheric correction is more critical. This fact is also confirmed by the radial gradients observed in the bias in $S\downarrow$ shown in LSA-SAF (2010b). Therefore, the MSG viewing zenith angle was one of the criteria for the classification.

The methodologies for obtaining the LAI also contain some differences. MSG-ET products obtain the LAI from the ECOCLIMAP database (Masson *et al.*, 2003). These are obtained by taking *in situ* maximum and minimum values of LAI and considering AVHRR NDVI series to impose seasonality per class cover. For Europe, monthly NDVI composites during the year 1997 produced by the DLR (Mucher *et al.*, 2001) are considered, and for the rest of the world, the International Geosphere-Biosphere Programme Data (IGBP) 1 km AVHRR NDVI composites from April 1992 until March 1993 (Belward *et al.*, 1999). However, GLDAS-ET take the LAI products derived at the University of Maryland (Myneni *et al.*, 2002), which are physically based and use the Moderate Resolution Imaging Spectroradiometer (MODIS) channels and scattering properties for the modeling. Alternatively, literature-based LAI are used in GLDAS-ET.

The NDVI was selected as second criterion for the classification, since it is one of the main inputs for one of the analyzed methodologies and it contributes to the seasonality of the data. Differences in the methods are expected to be higher for increasing NDVI. The position of the NDVI maximum (*t_max*) allows differentiating areas that have the peak in the $bias_{ET}$ in different seasons, such as the ones shown in Figure 2. The absolute value of the NDVI maximum (*NDVI_max*) allows differentiating areas that have different amplitude in the $bias_{ET}$.

Estimation of ET_b

The calculation of the ET_b in a daily base is given by:

$$ET_b = \Delta ET - bias_{ET} \quad (3)$$

where ΔET is the difference between MSG-ET and GLDAS-ET. The value of $bias_{ET}$ depends on the class assigned to every pixel based on the criteria previously mentioned which are elaborated in next sections.

Results

Classification Map

In order to produce the classification map the following criteria were taken into account. Figure 2 shows maximum bias approximately 2.5 and 5 mm under VZA of 48° and 65°. These data provide an indication of the rate at which the bias increases. Therefore, intervals of 10 in VZA were considered in the present work.

Sobrino and Raissouni (2000) proposed NDVI thresholds to distinguish between soil pixels (NDVI <0.2) and pixels of full vegetation (NDVI >0.5) obtained from AVHRR. These values were also used with the same purpose with other remote sensed sensors as it is explained in Sobrino *et al.* (2008b). In order to include also medium to high vegetated pixels, a reasonable NDVI value of 0.4 is taken in this work to distinguish between high and low vegetated pixels.

Due to differences in latitude, seasonal warmer periods arrive at different times in different areas and therefore the growing season is shifted. In order to take into account this effect and be able to generalize the method at other continents, the position of the *NDVI_max* was taken as a reference and two options were considered, *t_max* between April-September or outside that period. In order to be consistent with the ET_{actual} inputs of the proposed model, NDVI data were taken from the same source as the MSG-ET NDVI input. Figures 3 and 4 illustrate the criteria used for the classification, and Plate 1 the resulting classification map, generated at a resolution of approximately 1 km.

Estimation of Reference $bias_{ET}$

In order to obtain the bias in ET_{actual} for the different classes, four big areas covering the angle ranges of 40° to 50°, 50° to 60° and higher than 60° were selected, namely the Iberian Peninsula (classes LWH, LWL, LSH, and LSL according to Plate 1), Mid-South Germany (classes MWH, MWL, and MSH) plus Turkey (class MSL) and Mid-East Ukraine (classes HWH, HWL, HSH, and HSL), for which the difference between MSG-ET and GLDAS-ET was calculated per pixel and per class only in rainfed areas according to the GlobCover map. These calculations were carried out at the resolution of the GlobCover map (300 m), and in order to ensure homogeneity,

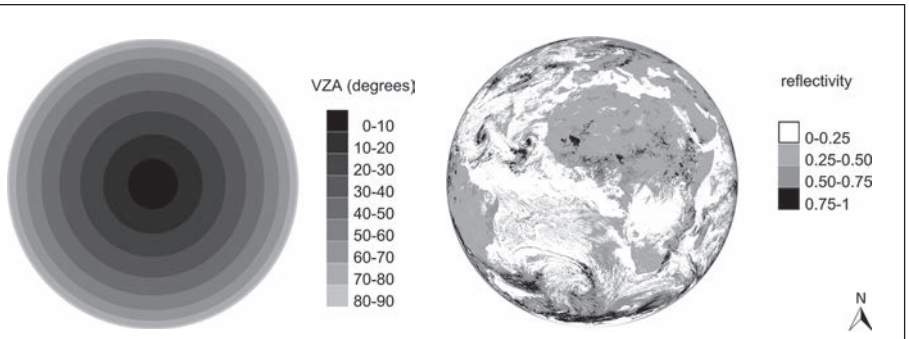

Figure 3. MSG field of view: (a) Viewing zenith angle (VZA), and (b) for reference, reflectivity image acquired in the visible spectrum.

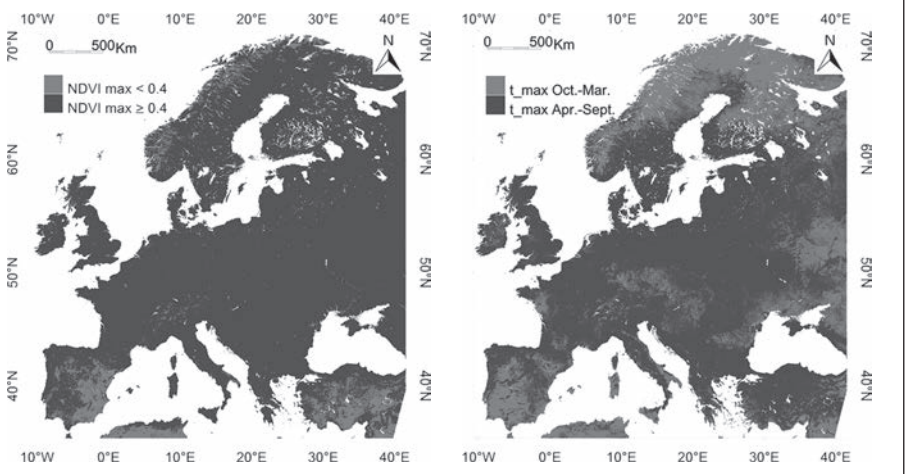

Figure 4. (a) *NDVI_max* during 1997, and (b) Season when *NDVI_max* occurs (*t_max*), calculated from the DLR data.

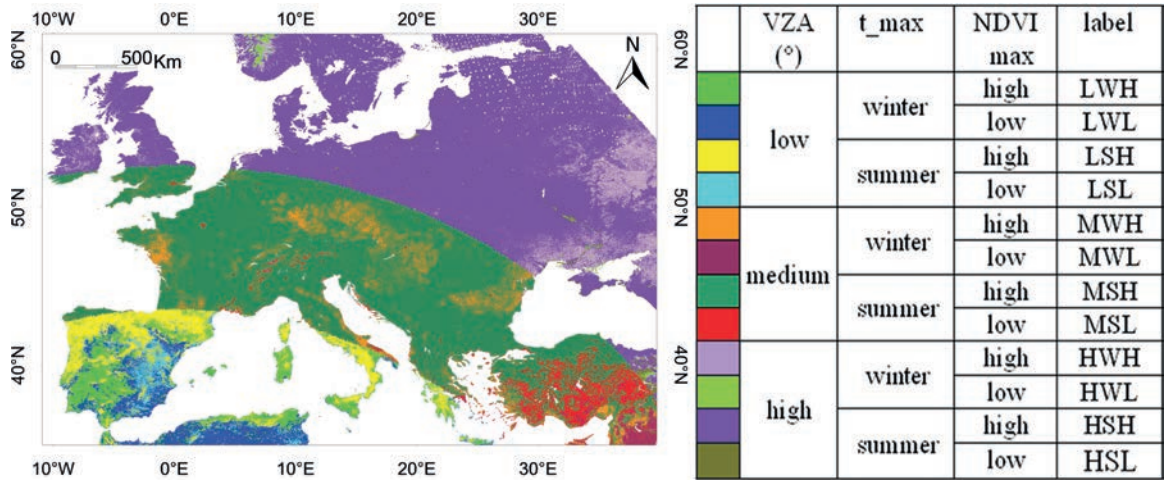

	VZA (°)	t_max	NDVI max	label
	low	winter	high	LWH
			low	LWL
		summer	high	LSH
			low	LSL
	medium	winter	high	MWH
			low	MWL
		summer	high	MSH
			low	MSL
	high	winter	high	HWH
			low	HWL
		summer	high	HSH
			low	HSL

Plate 1. Classification map of Europe for obtaining different $bias_{ET}$ and table defining the classes. Viewing zenith angles (VZA) are labeled as "low" (40° to 50°), "medium" (50° to 60°), and "high" (>60°). The season when NDVI maximum occurs is labeled as "winter" (October to March period) and "summer" (April to September period). The value of NDVI maximum is labeled as "high" (≥0.4) and "low" (<0.4). The label of every class corresponds to the combination of the first letter of these three sub-labels.

pixels were taken into account only when the surrounding pixels were also classified as rainfed in a 3 pixel by 3 pixel window. Figure 5 shows the mean values of the biases for the 12 classes obtained in Europe. These curves were smoothed by using moving averages of $\pm$ 2 days.

Figure 5 shows increasing amplitude in the bias with higher VZA, and differences in the profiles of the curves. Higher values of the bias are found when the *NDVI_max* is higher than 0.4, especially in summer periods. Moreover, the position of the peak of the bias is shifted somewhat when comparing classes with different *t_max* (see for example classes LWH and LSH).

Although some of the bias curves have similar patterns, and some of the classes are less abundant in the continent selected, all 12 biases have been kept in this analysis, in order to provide a general method that can be developed and applied in other regions of the globe, where other differences may arise and distribution of classes may change.

Calculation of ET_b

ET_b on a daily base was calculated following Equation 3 at a resolution of 1 km and rescaled to 5 arc-minutes (~10 km) for further comparison with other data. As an example, Figure 6a shows ET_b during 2008 in an irrigated pixel in Spain. Spring and summer periods show higher values of ET_b compared to the rest of the year. The accumulated ET_b during the year 2008 is also shown in Figure 6b in two irrigated pixels in Romania and Spain, where differences in accumulated ET_b are observed and may be explained by

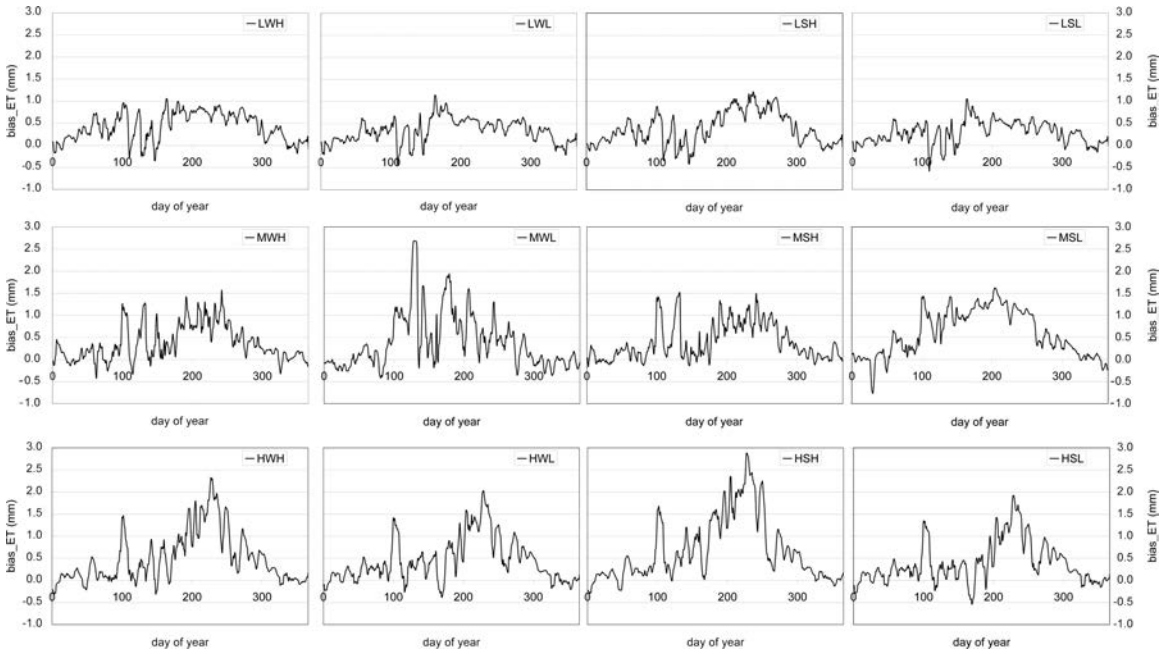

Figure 5. Bias between ET_{actual} products, MSG-ET, and GLDAS-ET, for rainfed pixels, calculated for the defined classes (see labels in Plate 1).

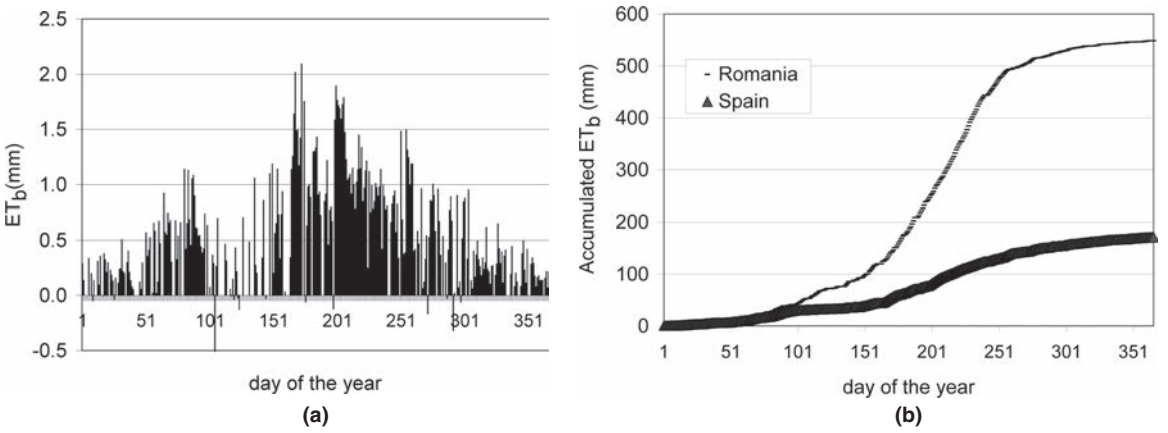

Figure 6. (a) Daily ET_b obtained in an irrigated pixel in Spain during the year 2008 with the proposed method, and (b) Accumulated ET_b in two irrigated pixels in Spain and Romania.

geographical and meteorological characteristics which, in the case of Romania, result in extensive irrigation practices (Virsta *et al.*, 2010).

Yearly ET_b at continental coverage were calculated by summing up the positive daily ET_b values. An additional mask was applied in order to filter the land covers that are out of the scope of this paper, which are forests, grasslands, shrub-lands, and sparse vegetation. The classes irrigated, rainfed, and mosaics of croplands and vegetation were used in this analysis. The GlobCover classification map was used for this purpose. The histogram of frequency of ET_b values is shown in Figure 7, where a relatively high amount of pixels have a value below 50 mm/year. These areas are considered non-irrigated croplands. Therefore, a reasonable value of 50 mm may be taken as the minimum value for which the proposed method is able to detect irrigation.

Figure 8 shows the ET_b image generated with the proposed method. The pixels labeled by the GlobCover map as irrigated or rainfed croplands, and pixels with mixed classes that include croplands, are plotted in the figure. Forests, grassland, shrublands, and sparse vegetation are masked and considered non-irrigated, as well as ET_b values below the defined threshold (50 mm/year). As an example, when ET_b country aggregated values are computed in Spain, Italy and Greece, they provide values of 23,000, 5,300, and 10,300 mm^3/year, which have the same order of magnitude than the ones provided by Mekonnen and Hoekstra (2011).

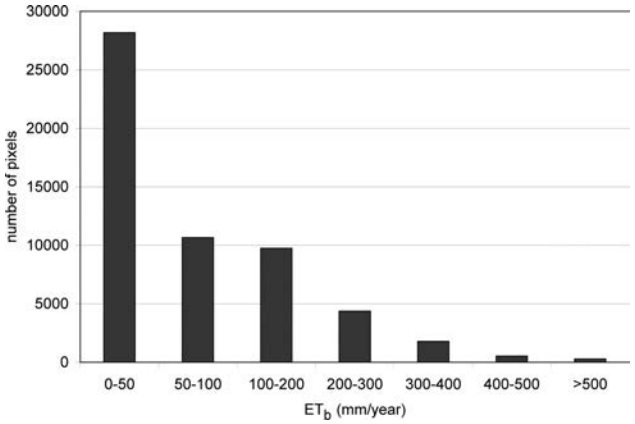

Figure 7. Yearly accumulated ET_b histogram in the region of Europe.

Accuracy of the Method

Accuracy assessment of the method was carried out in two ways, by evaluating the representativity of the defined bias and by analyzing the significance of the negative daily ET_b values that are obtained in some cases.

In order to evaluate the representativity of the defined biases, a similar analysis was carried out extending the reference areas to all rainfed croplands that belong to the same class in the classification map. The study was carried out at a coarser resolution (1 km), and in order to ensure homogeneity, pixels were taken into account only when the surrounding pixels were also classified as rainfed in a 3 pixel by 3 pixel window. The results (not shown here) provide similar mean bias curves for the classes LWH, LWL, LSH, MWH, MSH, and HWH with differences lower than 0.5 mm/day. Classes LSL and HSH provide lower values of the bias during summer, i.e., up to 1 mm/day. Classes MWL, HWL, and HSL are less abundant and are highly affected by the rescaling process, especially because the number of rainfed pixels is low and they are very scattered. Class MSL presents a different bias pattern when all scattered pixels outside the region of Turkey are included, with lower and negative amplitude in the summer time. The results show that for the most abundant classes, the reference bias may be considered as representative. However, the results also suggest how the bias in some classes may differ depending on the region where it is calculated; this mainly applies to less abundant classes and classes with higher VZA. In the present work, bearing in mind the application of the method, it seems reasonable to assign the bias obtained in the four defined windows to every class since they are obtained in cropland areas.

Moreover, Figure 6a shows that the method provides some negative ET_b values. In general, negative ET_b values are not physical and may occur due to noise in the inputs, especially at higher latitudes where the evapotranspiration rate is relatively low. Moreover, misclassification of pixels, e.g., forests, or non homogeneous classes may provide unrealistic results in areas for which the method is not appropriate. In order to evaluate the significance of these negative outputs, they were summed up during 2008 and combined with the yearly ET_{actual} calculated by accumulating the daily MSG-ET. Figure 9 shows the ratio between the accumulated negative ET_b and the accumulated ET_{actual}. The ratio is lower than 25 percent in most of the study area.

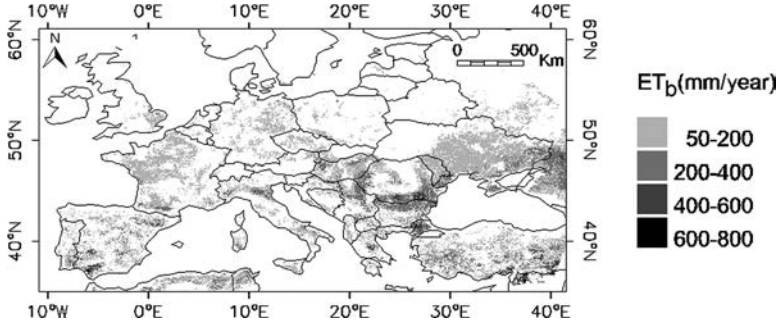

Figure 8. Yearly ET_b obtained with the proposed method in Europe during 2008 calculated in croplands according to the GlobCover map (irrigated and rainfed croplands, and mixed classes that include croplands).

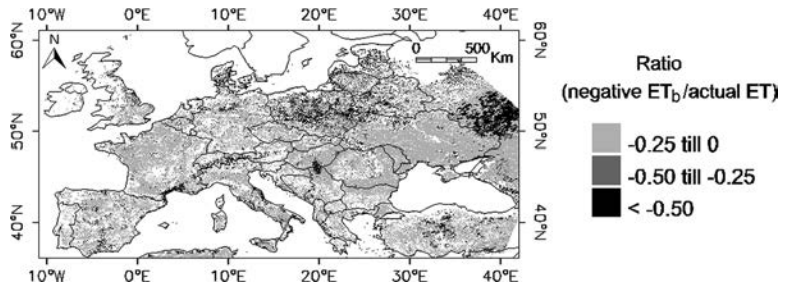

Figure 9. Ratio between the accumulated negative ET_b values obtained with the proposed method during 2008 and the accumulated ET_{actual} obtained from MSG-ET, calculated in croplands according to the GlobCover map (irrigated and rainfed croplands, and mixed classes that include croplands).

However, the significance of this ratio increases in some areas, such as next to mountains such as The Alps, or in higher latitudes in Poland or Denmark. Misclassification of pixels and high latitudes may explain the obtained results. Moreover, some regions in South France, Italy, and Hungary are relatively far from the areas where the reference biases were calculated. In these cases, the representativity of the bias may be lower and the resulting ET_b may be affected. Additionally, arid areas in Turkey or Spain with relatively low ET_{actual} rate are also prone to misclassification. Finally, the region of North Ukraine is located in the border of detection of MSG, and therefore the inaccuracies in ET_{actual} estimation may be higher due to the effects of the observation angle.

Test of the Method

The test of the proposed method was carried out using three approaches. The first one compared the irrigated area with the Global Map of Areas equipped for Irrigation (Siebert *et al.*, 2007) and the Global Irrigated Area Map (Thenkabail *et al.*, 2009b). Irrigated area aggregated to country level was also compared with the results given by Siebert *et al.* (2007) and Thenkabail et al. (2009b). Secondly, the ET_b volumes were compared with the results of Mekonnen and Hoekstra (2011). Finally ten-day ET_b estimates were compared at a pixel scale with *in situ* values of irrigation water in an irrigated cropland in Spain.

Irrigated Area Map

In order to compare the results with other products in terms of irrigated area, a binary classification was built for each map based on the following criteria. The label "irrigated" was assigned to the pixels in Figure 8 with ET_b higher than 50 mm/year. The rest were labeled as "non-irrigated". In the GMIA map (Siebert *et al.*, 2007) pixels were labeled as "irrigated" when a percentage of area equipped for irrigation was given; the rest were "non irrigated." Additionally, a threshold of 10 percent in the GMIA data was considered for labeling as "irrigated." Classes 1 to 8 in the aggregated GIAM map (Thenkabail *et al.*, 2009b) were labeled as "irrigated" and the rest as "non irrigated."

Table 2 shows the results obtained when assessing the accuracy of the generated map with respect to the other products. The overall accuracy is calculated by summing the number of pixels classified correctly and dividing by the total number of pixels. The kappa coefficient (Congalton and Green, 2009) is a more robust measure since it takes into account the agreement occurring by chance.

Table 2 shows a percentage of overlap of 72 percent when comparing with the map of Thenkabail *et al.* (2009b). A more detailed analysis (not shown here) illustrated that the disagreements are mainly due to pixels that the proposed method assigned to "irrigated" and were "non irrigated" in the reference map. This comparison provided a kappa of 0.109, which can be interpreted as a poor or very poor agreement (Monserud and Leemans, 1992).

The comparison with the map of Siebert *et al.* (2007) provided a percentage of overlap of 42 percent. The negative kappa means that the two maps agree less than would be expected by chance. The agreement improved when a threshold in the percentage of area equipped for irrigation is applied, which suggested that a less conservative binary classification would result in better agreements.

Irrigated Area per Country

The irrigated area was obtained for 2008 by considering the pixels with ET_b higher than 50 mm/year. The map by Ramankutty (2008) was used to weight the pixel size with the fraction of grid cell with crop. The results were aggregated to a country level and compared with the results given by Siebert *et al.* (2005) and Thenkabail *et al.* (2009b).

Figure 10 shows the results obtained for 13 countries in Europe, namely France, Spain, Germany, Poland, Italy, Romania, Greece, Bulgaria, Hungary, Portugal, Albania, Moldavia, and The Netherlands. The figure shows the agreement of the comparison in some countries, as it can be observed with values close to the 1:1 line. However, the

TABLE 2. OVERALL ACCURACY AND KAPPA COEFFICIENT OBTAINED WHEN COMPARING THE IRRIGATED AREA MAP OBTAINED WITH THE PROPOSED METHODOLOGY AND EXISTING PRODUCTS: THENKABAIL *ET AL.* (2009B), SIEBERT *ET AL.* (2007) AND SIEBERT *ET AL.* (2007) WITH A THRESHOLD OF 10 PERCENT IN THE AREA EQUIPPED FOR IRRIGATION

	Thenkabail *et al.* (2009b)	Siebert *et al.* (2007)	Siebert *et al.* (2007) (threshold = 10%)
Overall accuracy	72%	47%	72%
Kappa coefficient	0.109	−0.0064	0.1513

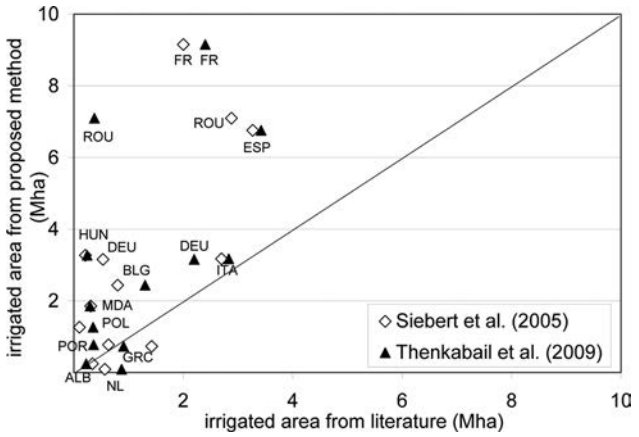

Figure 10. Comparison of the irrigated area provided by the proposed method and the country aggregated values given by Siebert *et al.* (2005) and Thenkabail *et al.* (2009b) in 13 countries in Europe. The figure also shows the 1:1 line. Country codes are: Albania (ALB), Bulgaria (BLG), France (FR), Germany (DEU), Greece (GRC), Hungary (HUN), Italy (IT), Moldova (MDA), The Netherlands (NL), Poland (POL), Portugal (POR), Romania (ROU), and Spain (ESP).

irrigated area in general is overestimated in the proposed method with respect to the values in the literature. The countries with higher disagreements are France, Romania, and Spain.

Different aspects may influence the differences that arise from the comparison. First, from a methodological point of view, the data provided by Siebert *et al.* (2005) are area equipped for irrigation obtained from statistical data bases and the data from Thenkabail *et al.* (2009b) are based on classification techniques, whereas the proposed method estimates the existence of irrigation based on physical processes that occur and using a threshold in the yearly ET_b. The year of the data that are used in the methods may also play a role, in this case the years 2000, 1999, and 2008, respectively, since irrigation areas may have changed and the meteorological conditions vary and therefore influence the inputs of the proposed method and also the approach of Thenkabail *et al.* (2009b). Moreover, the proposed method may lead to overestimation since it assumes that irrigation is met in the whole crop area within the pixel. Understanding the sub-pixel composition and heterogeneity, and the influence of the spatial resolution in estimating irrigated areas is analyzed in detail in Velpuri *et al.* (2009).

Finally, it is worth to mention that the literature shows discrepancies in the comparison of the two aforementioned existing datasets, which is explained in detail in Thenkabail *et al.* (2009b).

ET_b Map

This section compares the ET_b obtained in 2008, denoted by ROM in the following, with the blue water footprint (WF) values given by Mekonnen and Hoekstra (2011) in mm/year, named MH in the following.

Being aware that the two sources of data were obtained for different periods of time, an initial visual comparison was carried out in the region of Europe. In general terms, the position of the peaks in ET_b shown in MH were consistent with the ones provided by ROM, which were found in Greece and mid-south of Spain and Portugal, and north-east of Spain. Other relative maxima in MH in lower range of values appeared also in ROM, namely north and east of Italy, south of France, south of Ukraine, North of Africa and Turkey. However, ROM presented high values of ET_b in the regions of Romania, Serbia, and Hungary which were not described by MH. These areas are equipped for irrigation according to the Global Map of Irrigated areas from Siebert *et al.* (2007). In particular, the southern part of Romania and eastern-most tip of Serbia is called the Romanian Plain, and is known for its intensive irrigation (Virsta *et al.*, 2010).

From a quantitative point of view, the overlap between the two maps is 75 percent when taking a range of $\pm$ 50mm/year.

Comparison of ET_b with *in situ* Data

The area selected for the test is located in Barrax, Spain (39°03'N, 02° 06'W), which has been used for agricultural research for many years (Guanter *et al.*, 2007; Sobrino *et al.*, 2008a; Su *et al.*, 2008). The area is characterized by a flat morphology and large, uniform land use units. Differences in elevation range up to 2 m. The regional water table is about 20 to 30 m below the land surface. The region consists of approximately 65 percent dry land and 35 percent irrigated land with different agricultural fruits. In particular, the *in situ* data were provided by the local institution *Servicio de Asesoramiento de Riegos del Instituto Técnico Agronómico Provincial* (ITAP) in Albacete (Spain) (Montoro *et al.*, 2011), and consisted of volumes of irrigated water supplied to a corn field during the year 2009, corn being one of the dominant crops in the test area.

The comparison of ET_b with *in situ* data was carried out by using an Advanced Spaceborne Thermal Emission and Reflection Radiometer (ASTER) image in order to downscale the data. The ASTER image was acquired on the 18 July 2004 in the framework of the Spectra Barrax Campaign (SPARC). The visible and near infrared channels have a spatial resolution of 15 m, and they were used to compute the NDVI as an indicator of the amount of vegetation cover. Two areas which contained the corn field were selected, with dimensions around 6 km $\times$ 6 km and 13 km $\times$ 10 km, and a threshold of 0.4 was selected to define highly vegetated covers. Additionally, an NDVI threshold of 0.6 was set in order to analyze the influence in the results. Figure 11 shows the NDVI mask when using these two thresholds, together with the size of the areas of interest and the location of the corn field.

This test assumed that all crops with NDVI higher than the threshold behaved like the corn pivot, for which *in situ* irrigation data were available. The final result in the areas of interest was obtained multiplying the corn irrigation value by the percentage of fully vegetated cover taken from the NDVI mask.

Additionally ET_b was calculated following the proposed method between 10 July and 08 September, period for which MSG-ET products were available in the region. The daily ET_b was obtained only for the 89 percent of the days due to lack of data as previously explained.

Table 3 shows the comparison of the results by accumulating ET_b every ten days in the two areas using the two NDVI thresholds. Negative ET_b values obtained in some pixels of Area 2 summed up a total of 1.2 mm for the whole period and were not considered.

When comparing the modeled ET_b in Area 1 with *in situ* values in periods of ten days, the differences were not systematic and had positive and negative values, being higher

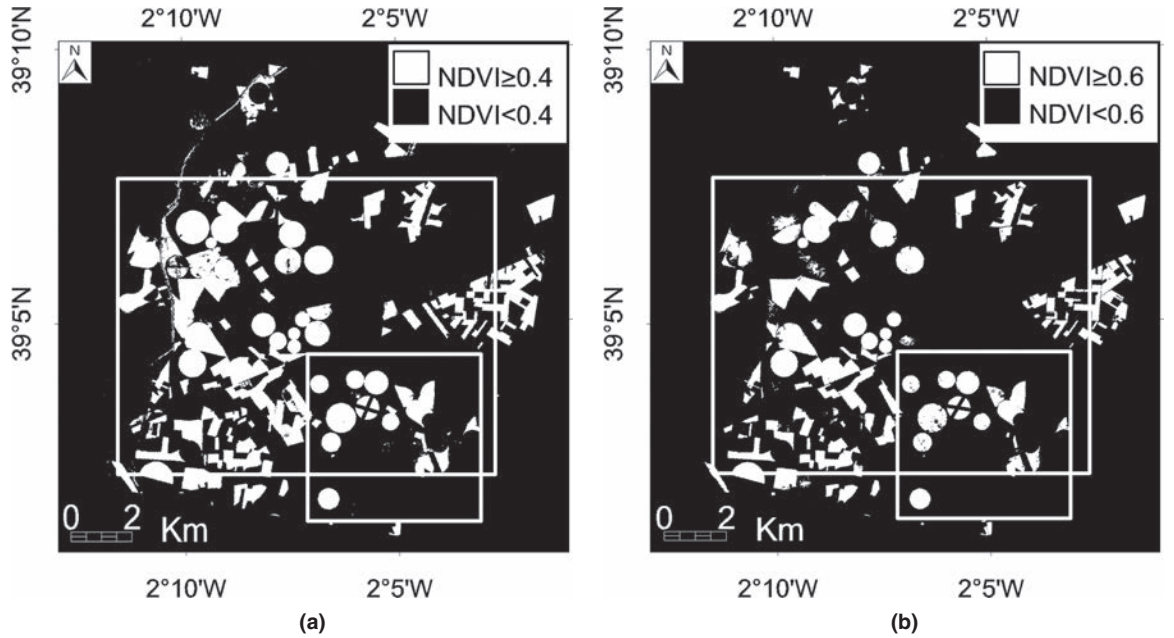

Figure 11. ASTER NDVI mask in the region of test in Spain with thresholds in (a) 0.4, and (b) 0.6. The size of the areas of study and the location of the corn field for which *in situ* data are available, are also indicated with rectangles and a cross respectively.

TABLE 3. ET_B VALUES OBTAINED IN THE TWO AREAS OF INTEREST BY USING THE MODEL PROPOSED IN THIS PAPER AND BY USING *IN SITU* DATA WITH NDVI THRESHOLDS OF 0.4 AND 0.6

	ET_b Area 1 (mm)			ET_b Area 2 (mm)		
10-days period number	method	in situ 04	in situ 06	method	in situ 04	in situ 06
1	10.4	13.5	11.5	15.3	20.9	14.6
2	15.7	11.6	9.9	21.5	18.0	12.6
3	11.3	13.6	11.5	16.9	21.0	14.7
4	10.2	9.7	8.2	13.5	15.0	10.5
5	7.3	7.7	6.6	11.7	12.0	8.4
6	7.8	13.6	11.5	11.9	21.0	14.7
total (% difference)	62.6	69.6 (10%)	59.2 (6%)	90.7	108.0 (16%)	75.4 (20%)

when the selected NDVI threshold was 0.4. Although individual values may present high percentages of discrepancy, the total value presented differences of 10 and 6 percent when NDVI threshold was 0.4 and 0.6, respectively. A similar pattern was observed in Area 2 with 16 and 20 percent of difference with respect to the *in situ* values, and noticing that the method slightly overestimated ET_b in the ten-day periods when the selected NDVI threshold was 0.6.

In this context, it is important to highlight that the *in situ* irrigation data were values discrete in time, whereas the model provided continuous ET_b daily values. This fact may explain the high discrepancies in some of the periods, since remote sensing observes the delayed effects of irrigation in terms of ET_{actual}, and *in situ* values are assigned to particular days.

Discussion

This section describes aspects to be taken into account when interpreting the method and the results obtained in this paper.

First, the proposed method is highly influenced by the inaccuracies of the inputs. In particular, the method may lead to errors due to the misclassification of rainfed pixels in the land-cover map input, since it is the base for the calculation of the reference bias of the proposed method. This fact is also affecting the forest, grasslands, shrublands, and sparse vegetation mask applied to generate the ET_b image. Other maps that define irrigated and rainfed areas and were developed specifically to describe croplands are the ones given by Thenkabail *et al.* (2009a and 2009b), and may be considered as alternative inputs for the proposed method. Moreover, the existence of data gaps in the MSG-ET inputs influences the daily assessments of ET_b and therefore the yearly accumulated value. In this work, a linear interpolation was carried out to fill in missing data and daily ET_{actual} values were not considered if the lack of data occurred during periods of one hour or longer, achieving a total of 94 percent of daily ET_b if the five month period May to September was considered. In general, a more accurate approach may be considered to incorporate those days in the calculations as well as to evaluate the relevance of not including them.

The bias-pattern and the classification constitute one of the main bases of the method. The classes and criteria selected are explained in the text. Nevertheless, other approaches may have been used based for example on climatic classifications or forcing parameters as shown by Roerink *et al.* (2003). In general, for the main classes the bias pattern defined was representative for the whole class. However, the bias of minority classes presented more variability, especially when the pixels were scattered.

The validation of the method presents some difficulties because of the unavailability of MSG-ET remote sensing data during the years analyzed in the existing literature. Moreover, water resources and irrigation are politically critical issues, and generally *in situ* quality data are difficult to access. In this context, this work shows the strength of a remote sensing-based method that allows locating and quantifying irrigation practices from an independent data set. The potential of using remote sensing techniques in this field was also described by Romaguera *et al.* (2010). Despite the lack of time coincident data for validation, this paper shows the comparison of ET_b volumes and irrigated area with existing methodologies and the differences and similarities were discussed.

Regarding the *in situ* test, different issues need to be mentioned. The NDVI image used for the threshold of fully vegetated covers was acquired in 2004 and is assumed to be valid for the year 2009 and static along the period of analysis. Changes in cover type may affect the results. Moreover, different crops may have different water requirements than corn and not all irrigation water supplied will be evapotranspired.

Finally, regarding the generalization of the method, areas where all production is irrigated and precipitation is too small for rainfed production may present difficulties for defining the reference bias due to the lack of rainfed areas. Although differences in the inputs MSG-ET and GLDAS-ET are also expected in this case, further research needs to be carried out to adapt the method and quantify ET_b. For these areas, the method described in Romaguera *et al.* (2010) may be sufficient. Moreover, the availability of MSG-ET input data at the moment of writing this paper, only allows calculating ET_b in Europe from January 2007 to date, and in Africa and part of South America from September 2009 to date. However, the main concept of the method proposed can be generalized and applied to other ET_{actual} data with wider spatial and time coverage, by using the recently available official MODIS eight-day, 1 km ET_{actual} products over the years 2000 to 2009. This issue constitutes one of the lines of further research for the authors.

Conclusions

This paper provided an innovative and relatively simple method to identify irrigated areas and blue evapotranspiration (ET_b), or evapotranspiration of irrigation water from the field. It was based on the comparison of the actual evapotranspiration (ET_{actual}) products from the remotely sensed Meteosat Second Generation (MSG) and model simulations from the Global Land Data Assimilation System (GLDAS), and the production of a spatially dependent bias. The method was able to detect irrigation when yearly values of ET_b were higher than 50 mm. Accuracy assessment showed that the method performed satisfactory for the majority of the study area (Europe). ET_b was produced in Europe for the year 2008. The comparison with the existing maps of irrigated area from Siebert *et al.* (2007) and Thenkabail *et al.* (2009b) provided a spatial match of 47 and 72 percent, respectively, with some overestimations on country aggregates. These differences can be associated to the sub-pixel heterogeneity and the influence of the spatial resolution in the analysis, as well as to methodological issues and data type. The spatial comparison of ET_b values with the ones given by Mekonnen and Hoekstra (2011) resulted in a 75 percent of overlap when a range of $\pm$ 50 mm was considered. Validation with point based *in situ* data showed a difference of less than 20 percent between measured and derived values. The proposed method provides an operational framework for quantifying and monitoring of irrigation at large scale and high temporal frequency. The approach can be easily generalized in time and space by defining the proper biases and analyzing the inputs of the models, at the continental scale of MSG data (including Africa), or by using the recently available global ET_{actual} products from the remotely sensed Moderate Resolution Imaging Spectroradiometer (MODIS) sensor.

Acknowledgments

The authors wish to thank the Land Surface Analysis Satellite Applications Facility (LSA-SAF) of the European Organisation for the Exploitation of Meteorological Satellites (EUMETSAT), as well as the European Space Agency (ESA) and the ESA GlobCover Project, led by MEDIAS-France, for providing the products used in this paper. The GLDAS data used in this study were acquired as part of the mission of NASA's Earth Science Division and archived and distributed by the Goddard Earth Sciences (GES) Data and Information Services Center (DISC).

The authors wish to thank the institution *Servicio de Asesoramiento de Riegos del Instituto Técnico Agronómico Provincial* (ITAP) in Albacete (Spain), for providing the *in situ* data used for the test of the proposed method. Moreover, the authors wish to thank the anonymous referees and Prasad Thenkabail, for their constructive remarks which have assisted us to improve the quality of the manuscript.

References

Allen, R., L.S. Pereira, D. Raes, and M. Smith, 1998. *FAO Irrigation and Drainage Paper n.56: Crop Evapotranspiration*, Food and Agriculture Organization, Rome, Italy.

Belward, A.S., J.E. Estes, and K.D. Kline, 1999. The IGBP/DIS Global 1-Km land-cover data set DISCover - A project Overview, *Photogrammetric Engineering & Remote Sensing*, 65(9): 1013–1020.

Chen, F., K. Mitchell, J. Schaake, Y.K. Xue, H.L. Pan, V. Koren, Q.Y. Duan, M. Ek, and A. Betts, 1996. Modeling of land surface evaporation by four schemes and comparison with FIFE observations, *Journal of Geophysical Research-Atmospheres*, 101:7251–7268.

Congalton, R.G., and Green, K. (2009). *Assessing the Accuracy of Remotely Sensed Data – Principles and Practices*, CRC Press, Taylor & Francis Group, Boca Raton, Florida, 183 p.

D'Urso, G., f. Vuolo, and c. De Michele, 2008. Remote sensing techniques to improve on farm irrigation efficiency, *Irrigation Australia*, 20-22 May, Melbourne, Australia.

Gellens-Meulenberghs, F., A. Arboleda, and N. Ghilain, 2007. Towards a continuous monitoring of evapotranspiration based on MSG data, *Proceedings of the IAHS Symposium on Remote Sensing for Environmental Monitoring and Change Detection*, Perugia, Italy, IAHS Press, Wallingford, ROYAUME-UNI.

Gowda, P.H., J.L. Chavez, P.D. Colaizzi, S.R. Evett, T.A. Howell, and J.A. Tolk, 2008.. ET mapping for agricultural water management: Present status and challenges, *Irrigation Science*, 26:223–237.

Guanter, L., V. Estelles, and J. Moreno, 2007. Spectral calibration and atmospheric correction of ultra-fine spectral and spatial resolution remote sensing data, Application to CASI-1500 data, *Remote Sensing of Environment*, 109:54–65.

Koren, V., J. Schaake, K. Mitchell, Q.Y. Duan, F. Chen, and J.M. Baker, 1999. A parameterization of snowpack and frozen

ground intended for NCEP weather and climate models, *Journal of Geophysical Research-Atmospheres*, 104:19569–19585.

LSA-SAF, 2010a. *LSA-SAF Product User Manual, Evapotranspiration (ET)*, The EUMETSAT Network of Satellite Application Facilities, Document Number: SAF/LAND/RMI/PUM_MET/2.3.

LSA-SAF, 2010b. LSA-SAF validation report, Products LSA-16 (MET), LSA-17 (DMET), *The EUMETSAT Network of Satellite Application Facilities*, Document Number: SAF/LAND/RMI/VR/0.6.

Masson, V., J.L. Champeaux, F. Chauvin, C. Meriguet, and R. Lacaze, 2003. A global database of land surface parameters at 1-km resolution in meteorological and climate models, *Journal of Climate*, 16:1261–1282.

Mekonnen, M.M., and A.Y. Hoekstra, 2010. A global and high-resolution assessment of the green, blue and grey water footprint of wheat, Value of Water Research Report No.42, *Value of Water Research Report No.42*, Delft, The Netherlands: UNESCO-IHE.

Mekonnen, M.M., and A.Y. Hoekstra, 2011. National water footprint accounts: The green, blue and grey water footprint of production and consumption, *Value of Water Research Report Series, No.50,* Delft, The Netherlands: UNESCO-IHE.

Monserud, R.A., and R. Leemans, 1992. Comparing Global Vegetation Maps with the Kappa-Statistic, *Ecological Modelling*, 62: 275–293.

Montoro, A., P. Lopez-Fuster, and E. Fereres, 2011. Improving on-farm water management through an irrigation scheduling service, *Irrigation Science*, 29:311–319.

Mucher, C.A., J.L. Champeaux, K.T. Steinnocher, S. Griguolo, K. Wester, C. Heunks, W. Winiwater, F.P. Kressler, J.P. Goutorbe, B. ten Brink, V.F. Van Katwijk, O. Furberg, V. Perdigao, and G.J.A. Nieuwenhuis, 2001. Development of a consistent methodology to derive land cover information on an European scale from remote sensing for environmental modeling, *The PELCOM Report: Report 6*, Center for Geo-Information (CGI), Alterra, Wageningen, The Netherlands, p. 160.

Myneni, R.B., S. Hoffman, Y. Knyazikhin, J.L. Privette, J. Glassy, Y. Tian, Y. Wang, X. Song, Y. Zhang, G.R. Smith, A. Lotsch, M. Friedl, J.T. Morisette, P. Votava, R.R. Nemani, and S.W. Running, 2002. Global products of vegetation leaf area and fraction absorbed PAR from year one of MODIS data, *Remote Sensing of Environment*, 83:214–231.

NWC-SAF, 2010. Algorithm theoretical basis document for SAFNWC/PPS "Cloud Mask" (CMPGE01 v3.0-patch1), *The EUMETSAT Network of Satellite Application Facilities*, Document Number SAF/NWC/CDOP/SMHI-PPS/SCI/ATBD/1.

Ozdogan, M., M. Rodell, H.K. Beaudoing, and D.L. Toll, 2010. Simulating the effects of irrigation over the United States in a land surface model based on satellite-derived agricultural data, *Journal of Hydrometeorology*, 11:171–184.

Ramankutty, N., A.T. Evan, C. Monfreda, and J.A. Foley, 2008. Farming the planet: 1. Geographic distribution of global agricultural lands in the year 2000, *Global Biogeochemical Cycles*, 22(1), doi:1010.1029/2007GB002952.

Rodell, M., P.R. Houser, U. Jambor, J. Gottschalck, K. Mitchell, C.J. Meng, K. Arsenault, B. Cosgrove, J. Radakovich, M. Bosilovich, J.K. Entin, J.P. Walker, D. Lohmann, and D. Toll, 2004. The global land data assimilation system, *Bulletin of the American Meteorological Society*, 85:381–394.

Roerink, G.J., M. Menenti, W. Soepboer, and Z. Su, 2003. Assessment of climate impact on vegetation dynamics by using remote sensing, *Physics and Chemistry of the Earth*, 28:103–109.

Romaguera, M., A.Y. Hoekstra, Z. Su, M.S. Krol, and M.S. Salama, 2010. Potential of using remote sensing techniques for global assessment of water footprint of crops, *Remote Sensing*, 2(4): 1177–1196.

Siebert, S., and P. Döll, 2010. Quantifying blue and green virtual water contents in global crop production as well as potential production losses without irrigation, *Journal of Hydrology*, 384: 198–217.

Siebert, S., P. Döll, S. Feick, J. Hoogeveen, and K. Frenken, 2007. *Global Map of Irrigation Areas*, version 4.0.1. Johann Wolfgang Goethe University, Frankfurt am Main, Germany / Food and Agriculture Organization of the United Nations, Rome, Italy.

Siebert, S., P. Döll, J. Hoogeveen, J.M. Faures, K. Frenken, and S. Feick, 2005. Development and validation of the global map of irrigation areas, *Hydrology and Earth System Sciences*, 9:535–547.

Sobrino, J.A., J.C. Jimenez-Munoz, G. Soria, M. Gomez, A.B. Ortiz, M. Romaguera, M. Zaragoza, Y. Julien, J. Cuenca, M. Atitar, V. Hidalgo, B. Franch, C. Mattar, A. Ruescas, L. Morales, A. Gillespie, L. Balick, Z. Su, F. Nerry, L. Peres, and R. Libonati, 2008a. Thermal remote sensing in the framework of the SEN2FLEX project: Field measurements, airborne data and applications, *International Journal of Remote Sensing*, 29: 4961–4991.

Sobrino, J.A., J.C. Jimenez-Munoz, G. Soria, M. Romaguera, L. Guanter, J. Moreno, A. Plaza, and P. Martinez, 2008b. Land surface emissivity retrieval from different VNIR and TIR sensors, *IEEE Transactions on Geoscience and Remote Sensing*, 46(2):316–327.

Sobrino, J.A., and N. Raissouni, 2000. Toward remote sensing methods for land cover dynamic monitoring: Application to Morocco, *International Journal of Remote Sensing*, 21:353–366.

Su, Z., W. Timmermans, A. Gieske, L. Jia, J.A. Elbers, A. Olioso, J. Timmermans, R. Van Der Velde, X. Jin, H. Van Der Kwast, F. Nerry, D. Sabol, J.A. Sobrino, J. Moreno, and R. Bianchi, 2008. Quantification of land-atmosphere exchanges of water, energy and carbon dioxide in space and time over the heterogeneous Barrax site, *International Journal of Remote Sensing*, 29: 5215–5235.

Thenkabail, P., G.J. Lyon, H. Turral, and C.M. Biradar, 2009a. *Remote Sensing of Global Croplands for Food Security*, CRC Press- Taylor and Francis Group, Boca Raton, London, New York, 556 p.

Thenkabail, P.S., C.M. Biradar, P. Noojipady, V. Dheeravath, Y.J. Li, M. Velpuri, M. Gumma, O.R.P. Gangalakunta, H. Turral, X.L. Cai, J. Vithanage, M.A. Schull, and R. Dutta, 2009b, Global irrigated area map (GIAM), derived from remote sensing, for the end of the last millennium, *International Journal of Remote Sensing*, 30:3679–3733.

Thenkabail, P.S., P. Gangadhara Rao, T. Biggs, M. Krishna, and H. Turral, 2007. Spectral matching techniques to determine historical land use/land cover (LULC) and irrigated areas using time series AVHRR Pathfinder datasets in the Krishna River basin, India, *Photogrammetric Engineering & Remote Sensing*, 73(9):1029–1040.

UCLouvain, and ESA, 2011. *GlobCover 2009*, Products description and validation report, 18 February 2008, European Space Agency.

Velpuri, N.M., P.S. Thenkabail, M.K. Gumma, C. Biradar, V. Dheeravath, P. Noojipady, and L. Yuanjie, 2009. Influence of resolution in irrigated area mapping and area estimation, *Photogrammetric Engineering & Remote Sensing*, 75(12):1383–1395.

Virsta, A., I. Giurma, S. Oancea, R. Sofronie, and I. Craciun, 2010. *Efecte ale Insulelor de Caldura in Climatologie, Medicina si Inginerie*, Editura Noua, 186 p.